PCCP

ROYAL SOCIETY OF CHEMISTRY

PAPER

View Article Online
View Journal | View Issue

Check for updates

Cite this: *Phys. Chem. Chem. Phys.*, 2022, **24**, 10263

The solution structures and relative stability constants of lanthanide–EDTA complexes predicted from computation†

Ravi D. O'Brien, Thomas J. Summers, Danil S. Kaliakin and David C. Cantu *

Ligand selectivity to specific lanthanide (Ln) ions is key to the separation of rare earth elements from each other. Ligand selectivity can be quantified with relative stability constants (measured experimentally) or relative binding energies (calculated computationally). The relative stability constants of EDTA (ethylenediaminetetraacetic acid) with La^{3+}, Eu^{3+}, Gd^{3+}, and Lu^{3+} were predicted from relative binding energies, which were quantified using electronic structure calculations with relativistic effects and based on the molecular structures of Ln–EDTA complexes in solution from density functional theory molecular dynamics simulations. The protonation state of an EDTA amine group was varied to study pH ~7 and ~11 conditions. Further, simulations at 25 °C and 90 °C were performed to elucidate how structures of Ln–EDTA complexes varying with temperature are related to complex stabilities at different pH conditions. Relative stability trends are predicted from computation for varying Ln^{3+} ions (La, Eu, Gd, Lu) with a single ligand (EDTA at pH ~11), as well as for a single Ln^{3+} ion (La) with varying ligands (EDTA at pH ~7 and ~11). Changing the protonation state of an EDTA amine site significantly changes the solution structure of the Ln–EDTA complex resulting in a reduction of the complex stability. Increased Ln–ligand complex stability is correlated to reduced structural variations in solution upon an increase in temperature.

Received 4th March 2022,
Accepted 1st April 2022

DOI: 10.1039/d2cp01081j

rsc.li/pccp

Published on 05 April 2022. Downloaded by University of Nevada - Reno on 5/20/2022 1:02:28 AM.

1. Introduction

The stability of lanthanide (Ln) ligand complexes in solution is relevant to purifying rare earth elements since complexation is needed to separate Ln^{3+} ions from each other in solution. The selectivity of a ligand to a particular Ln^{3+} ion compared to other Ln^{3+} ions determines the viability of Ln–Ln solvent extraction,[1,2] and it can be quantified by comparing the relative stability of a ligand to different Ln^{3+} ions. Ln–ligand complex stability can be determined experimentally with stability constant measurements,[3] or computationally with binding energy calculations.[4–7] Relative binding energies can be compared to relative stability constants and be used to predict ligand selectivity to a particular Ln^{3+} ion.

Changes in solution pH are used in rare earth separations to drive Ln extraction. For example, after the solvent extraction process, which transfers the desired Ln^{3+} ion to the organic phase as a Ln^{3+}–ligand complex, the Ln^{3+} ion is stripped to recycle the ligand that remains in the organic phase and concentrate the Ln^{3+} ion in the new aqueous phase.[8,9] The stripping process usually involves the addition of acid to unbind the Ln^{3+}–ligand complex. The Ln–ligand unbinding behavior in acidic conditions with protic ligands is well characterized at the process level; however, much remains to be resolved at a molecular scale regarding how solution pH affects Ln–ligand complex stability, and ultimately how solution pH affects ligand selectivity to particular Ln^{3+} ions.

Ethylenediaminetetraacetic acid (EDTA) is an ion chelator with six Brønsted acidic sites (four carboxylate, two amine) that change protonation state according to the solution pH. The stability constants of EDTA to most Ln^{3+} ions are known, and for some Ln^{3+} ions these constants are available for different protonation states.[3] Therefore, Ln^{3+}–EDTA complexes are ideally suited to develop a computational protocol that calculates relative Ln–ligand binding energies and identifies how pH affects the structure of Ln–ligand complexes in solution and their relative binding energies.

In order to calculate the relative binding energies of a ligand to Ln^{3+} ions, the molecular structures of Ln^{3+}–ligand complexes must be resolved. In solution, this is challenging due to the high number of degrees of freedom and conformations of a Ln/ligand/anion/solvent system.[10] In our previous work, we

Department of Chemical and Materials Engineering, University of Nevada, Reno, Reno, NV 89557, USA. E-mail: dcantu@unr.edu

† Electronic supplementary information (ESI) available: Discussion on binding energy calculations; energies of species used in binding energy calculations; root mean square distance analysis; plots of energy *vs.* simulation frame. See DOI: https://doi.org/10.1039/d2cp01081j

Published on 05 April 2022. Downloaded by University of Nevada - Reno on 5/20/2022 1:02:28 AM.

reported a computational protocol, based on density functional theory (DFT) *ab initio* molecular dynamics (AIMD) simulations that predicted the solution structure of the Eu^{3+}–EDTA complex within 0.05 Å of experimental measurements, including the number water molecules coordinated to the Eu^{3+} ion and ion coordination number.[11] In this work, the same DFT AIMD protocol is applied to determine the 25 °C solution structures of La^{3+}, Gd^{3+}, and Lu^{3+} complexes with EDTA at a protonation state corresponding to pH ~11, and that of La^{3+} complexed with EDTA at a protonation state corresponding to pH ~7. Relative binding energies, which are calculated based on the resolved complex structures in solution, are compared to experimental stability constants to identify a computational approach that can predict the selectivity of a ligand to a particular Ln^{3+} ion. In addition, AIMD simulations of the La–EDTA complexes at both pH values, and the Lu–EDTA complex, are performed at 90 °C to determine how Ln–ligand structural variation with temperature and pH relate to Ln–ligand complex stability.

2. Computational methods

Electronic structure calculations with relativistic effects (Section 2.1) were used to calculate binding energies based on the solution structures of Ln–ligand complexes that were resolved with DFT AIMD simulations (Section 2.2).

Ln–ligand binding energies (*BE*) were calculated using two thermodynamic integration schemes: (i) for a given ligand and varying Ln^{3+} ions, and (ii) for a given Ln^{3+} ion and varying ligands. Eqn (1) shows the thermodynamic integration to calculate Ln–ligand binding energies for a given ligand and varying Ln^{3+} ion:

$$BE_{[\mathrm{Ln\text{–}ligand}\cdot(H_2O)_n]^p} = E_{[\mathrm{Ln\text{–}ligand}\cdot(H_2O)_n]^p} - E_{Ln^{3+}} - E_{[\mathrm{ligand}]^{(p-3)}} - n\cdot E_{\mathrm{water}} \quad (1)$$

where n is the number of water molecules coordinated to the Ln^{3+} ion in the Ln–ligand complex and p is the charge of the Ln–ligand complex. At pH ~11 EDTA is completely unprotonated ($EDTA^{4-}$) while at pH ~7 EDTA has one proton ($HEDTA^{3-}$), resulting in Ln–EDTA complexes with an overall charge of −1 and 0, respectively. In this work the Ln ions are always in the +III oxidation state (Ln^{3+}), their most common state in solution. Eqn (2) shows the thermodynamic integration to calculate Ln–ligand binding energies for a given Ln^{3+} ion and varying ligand:

$$BE_{[\mathrm{Ln\text{–}ligand}\cdot(H_2O)_n]^p} = E_{[\mathrm{Ln\text{–}ligand}\cdot(H_2O)_n]^p} - E_{[\mathrm{Ln}\cdot(H_2O)_m]^{3+}} - E_{[\mathrm{ligand}]^{(p-3)}} - (m-n)\cdot E_{\mathrm{water}} \quad (2)$$

where m is the number of water molecules in the Ln^{3+} aqua ion without a ligand.

The main difference between the two thermodynamic integration schemes is that in eqn (1) the energy of the Ln^{3+} ion is calculated without any explicit solvent molecules, while in eqn (2) the energy of the Ln^{3+} ion is calculated as that of the Ln^{3+} aqua ion with coordinated water molecules. It was observed that using two different thermodynamic integration schemes rather than a single thermodynamic integration scheme provides better predictions for their respective cases: a given ligand (varying Ln^{3+} ion) and a given Ln^{3+} ion (varying ligand); see additional discussion in the ESI,† which also includes discussion regarding the use of relative binding energies instead of relative free binding energies.

The free energies of binding (ΔG^{bind}) from experiment were calculated from the measured stability constants ($\log(K)$) as shown in eqn (3):

$$\log(K) = \frac{\Delta G^{\mathrm{bind}}}{\ln(10)RT} \quad (3)$$

where R is the ideal gas constant and T is the temperature. Relative experimental free energies of binding were compared to relative calculated binding energies (*BE*), with the energies of the $[La^{3+}\text{–}EDTA^{4-}\cdot(H_2O)_n]^-$ complex as a reference point. Eqn (4) shows the absolute error ($\varepsilon_{\mathrm{exp\text{-}comp}}$) between experiment and computation:

$$\varepsilon_{\mathrm{exp\text{-}comp}} = \left| \frac{\Delta G^{\mathrm{bind}}_{[\mathrm{Ln-ligand}\cdot(H_2O)_n]^p}}{\Delta G^{\mathrm{bind}}_{[La^{3+}-EDTA^{4-}\cdot(H_2O)_n]^-}} - \frac{BE^{\mathrm{bind}}_{[\mathrm{Ln-ligand}\cdot(H_2O)_n]^p}}{BE^{\mathrm{bind}}_{[La^{3+}-EDTA^{4-}\cdot(H_2O)_n]^-}} \right| \times 100 \quad (4)$$

The binding energies, from experiment and computation, of the $[La^{3+}\text{–}EDTA^{4-}\cdot(H_2O)_n]^-$ complex were chosen as the reference point to reduce underestimating the relative error between experiment and computation. Since relative values are being compared, the magnitude of the absolute value of the reference changes the relative energies, *i.e.*, if the reference point has the smallest magnitude, then the errors are larger, whereas if the reference point has the largest magnitude, then the errors are artificially smaller. La appears at the start of the Ln series and has the smallest magnitude in binding energy values for a given ligand, so it is the most appropriate reference point to not underestimate the error between experiment and computation.

2.1. Binding energies from electronic structure calculations with relativistic effects

The energies of each species in eqn (1) and (2) were calculated with all-electron single-point energy calculations, as performed in our previous work, where we calculated the acidity constants of Ln aqua ions.[12] All energy calculations were done with the M06 functional, a relativistic second order Douglas–Kroll–Hess (DKH2) Hamiltonian,[13,14] segmented all-electron relativistically contracted (SARC) basis set[15] for the Ln atoms, and the minimally augmented[16] ma-def2-TZVPP basis set[17,18] for ligand and water atoms. Studies demonstrate that the M06 functional is a reliable choice for the calculations of thermodynamic properties in broad variety of chemical systems,[19] including the Ln-containing molecules and Ln complexes.[20,21] Relativistic effects are required for accurate calculations with Ln elements.[22] Thus, the DKH and SARC basis set have been used with lanthanides.[23–25] Another study demonstrated that the ma-def2-TZVP basis set containing

 This journal is © the Owner Societies 2022

Published on 05 April 2022. Downloaded by University of Nevada - Reno on 5/20/2022 1:02:28 AM.

diffuse functions improved the prediction of Ln–ligand binding energies when compared to the smaller 6-31+G* basis set.[5]

The ligand and water molecules were optimized with the M06 functional[26] and the cc-pVTZ basis set[27] to obtain the molecular coordinates for the energy calculation in the thermodynamic integration. The molecular coordinates of the Ln–ligand complexes were obtained from AIMD simulations (Section 2.2).

In all calculations, an implicit water solvent model (conductor-like polarizable continuum model) was used.[28] All electronic structure calculations were done with ORCA v4.1.2,[29] using the resolution of identity chain of sphere (RIJCOSX)[30] to improve efficiency. The "Grid7" and "GridX7" grids were used to improve accuracy.

2.2. Solution structures from *ab initio* molecular dynamics simulations

In our previous work, an $[Eu^{3+}–EDTA^{4-}]^{-}$ complex structure was placed in the center of a 17.5 Å × 17.5 Å × 17.5 Å periodic box and solvated with explicit water molecules and a Na^{+} ion to neutralize the charge. An AIMD protocol that includes high temperature MD and simulated annealing to identify a minimum of complex solution structure in a large conformational space was followed. As a result, the solution structure of the complex was identified as $[Eu^{3+}–EDTA^{4-}\cdot(H_2O)_3]^{-}$, with three water molecules directly coordinating to the Eu^{3+} ion, the four carboxylate groups coordinating in a monodentate fashion, and both amine nitrogen atoms coordinating to the Eu^{3+} ion, the same solution structure previously resolved from experiment.[31,32]

Using the optimized structure of the $[Eu^{3+}–EDTA^{4-}\cdot(H_2O)_3]^{-}$ complex in basic conditions in solution from our previous work,[11] we replaced the Eu^{3+} ion with a La^{3+}, Gd^{3+}, and Lu^{3+} ion in independent simulation boxes, and performed AIMD simulations of the periodic box with explicit water molecules to resolve the solution structures of the Ln–EDTA (La, Eu, Gd, Lu) complexes at pH ~ 11. In addition, the structure of the $[La^{3+}–HEDTA^{3-}\cdot(H_2O)_n]^{0}$ complex at pH ~ 7 was determined by adding a proton to an amine group in the equilibrated structure of the $[La^{3+}–EDTA^{4-}\cdot(H_2O)_3]^{-}$ complex. As the solvent conformations were already equilibrated, in this work the focuses of the AIMD simulations were to refine the ligand conformation, characterize $Ln^{3+}–O_{WATER}$, $Ln^{3+}–O_{EDTA}$, and $Ln^{3+}–N_{EDTA}$ coordination bonds, determine the number of water molecules that remain directly coordinated to the Ln^{3+} ion, and sample equilibrium configurations of the complexes in solution at 25 °C and 90 °C.

AIMD simulations in this work were performed in the NVT ensemble (constant volume and temperature), with a 1.0 fs time step, at 25 °C or 90 °C, to obtain at least 10 ps of equilibrated trajectory. The AIMD simulations at 90 °C were performed as in our previous work,[33] by taking an equilibrated frame at 25 °C and performing an NVT simulation at 90 °C until at least ~10 ps of equilibrated trajectory were sampled. The analysis of radial distribution functions (RDFs), coordination numbers (CNs), and root mean square deviations (RMSDs, see SI) to ideal geometries of the studied systems was done for equilibrated parts of the trajectories that corresponded to at least ~10 ps. Plots of the potential energies, which were used to determine equilibration of the AIMD trajectories appear in the SI. DFT AIMD simulations were performed within the PBE/LnPP1 GTH level of theory,[34,35] as implemented in the CP2K v5.1 package.[36] Core electrons were modeled with norm-conserving GTH pseudopotentials, while valence electrons were treated with polarizable double-zeta quality basis sets.[37] We used LnPP1 pseudopotentials and basis sets for the lanthanides, which include the *f* electrons in the valence shell.[35] The long-range electrostatics terms were calculated with an additional plane wave basis set, with a 500 Ry cutoff for La, Eu, and Gd, and a 1000 Ry cutoff of Lu. Grimme's dispersion correction (DFT-D3)[38] was used to account for van der Waals interactions with a 6.0 Å radius. All systems containing La^{3+} and Lu^{3+} had singlet multiplicity, Eu^{3+} had septet multiplicity, and Gd^{3+} had an octet multiplicity. This DFT and AIMD protocol was previously shown to result in structures of the Ln aqua ions, and the $[Eu^{3+}–EDTA^{4-}\cdot(H_2O)_3]^{-}$ complex, with Ln–O and Eu–N distances within 0.05 Å of those measured with extended X-ray absorption fine structure spectroscopy.[11,39]

The coordinates of Ln–ligand complex, used for binding energy calculations (Section 2.1), were optimized in the solution phase by the following protocol in the full explicit solvent simulation box: starting from an AIMD equilibrated frame at 25 °C, a simulated annealing to ~0 K was performed (typically ~2000 MD steps), followed by a final geometry optimization.

3. Results and discussion

3.1. Solution structures of Ln–EDTA complexes

Fig. 1 shows the resolved solution structures at 25 °C of La^{3+}, Eu^{3+}, Gd^{3+}, and Lu^{3+} complexed with $EDTA^{4-}$, the protonation state of EDTA at pH ~ 11. The structure of the $[Eu^{3+}–EDTA^{4-}\cdot(H_2O)_3]^{-}$ complex was resolved in our previous work,[11] but is discussed here for comparison. The structures of the $[La^{3+}–EDTA^{4-}\cdot(H_2O)_3]^{-}$ and $[Gd^{3+}–EDTA^{4-}\cdot(H_2O)_3]^{-}$ complexes are very similar to that of the $[Eu^{3+}–EDTA^{4-}\cdot(H_2O)_3]^{-}$ complex such that the four carboxylates bound in a monodentate fashion, both nitrogen atoms buckled in to form coordination bonds with the Ln^{3+} ion, and has three coordinated water molecules to give a total coordination number of 9. The $[Lu^{3+}–EDTA^{4-}\cdot(H_2O)_2]^{-}$ complex had the same ligand conformation, except that two water molecules remained coordinated to the Lu^{3+} ion instead of three, resulting in a total coordination number of 8. These findings are in agreement with results from a classical molecular dynamics study examining the chelation of $EDTA^{4-}$ with La^{3+}, Eu^{3+}, and Lu^{3+}.[40]

Fig. 1 illustrates the structure of the La^{3+} ion complexed with the protonated $HEDTA^{3-}$ molecule. Unlike the $[La^{3+}–EDTA^{4-}\cdot(H_2O)_3]^{-}$ structure, in the $[La^{3+}–HEDTA^{3-}\cdot(H_2O)_4]^{0}$ complex the nitrogen of the protonated amine group did not coordinate with the La^{3+} ion, and instead, an additional fourth water molecule bound to the La^{3+} ion to maintain a 9-coordinate structure. Therefore, solution pH and subsequent change in

Published on 05 April 2022. Downloaded by University of Nevada - Reno on 5/20/2022 1:02:28 AM.

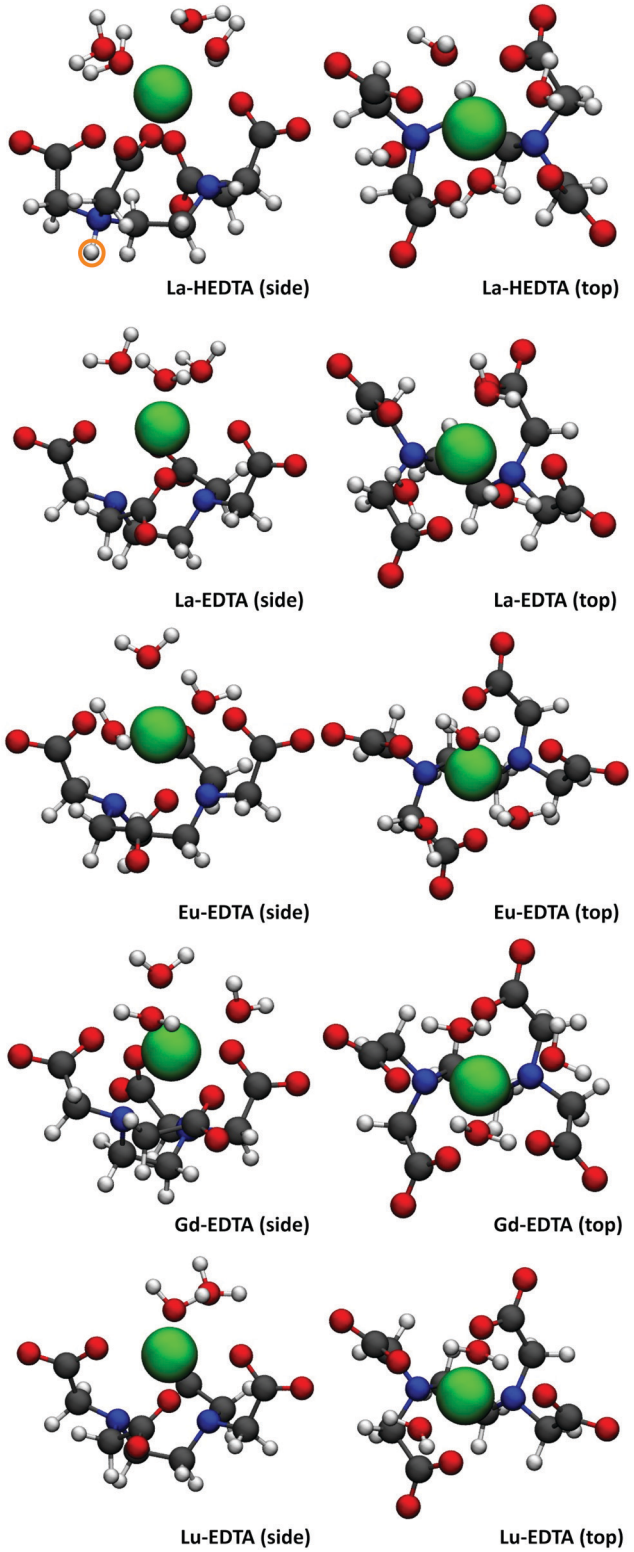

Fig. 1 Side views (left) and top views (right) of the optimized solution structures of the $[La^{3+}–HEDTA^{3-}\cdot(H_2O)_4]^0$, $[La^{3+}–EDTA^{4-}\cdot(H_2O)_3]^-$, $[Eu^{3+}–EDTA^{4-}\cdot(H_2O)_3]^-$, $[Gd^{3+}–EDTA^{4-}\cdot(H_2O)_3]^-$, and $[Lu^{3+}–EDTA^{4-}\cdot(H_2O)_2]^-$ complexes at 25 °C, in descending order. Only molecules coordinated to the Ln^{3+} ion are shown for clarity; however, all structures are in solution and were determined in a periodic box with explicit water molecules. Ln^{3+} ions in green, carbon atoms in gray, oxygen atoms in red, nitrogen atoms in blue, and hydrogen atoms in white. An orange circle highlights the protonation state difference between $HEDTA^{3-}$ and $EDTA^{4-}$, which correspond to pH ~ 7 and pH ~ 11, respectively.

EDTA protonation state changes the coordination structure of Ln–EDTA complexes.

Radial distribution functions (RDFs) were computed for each complex to illustrate the frequency of carbon, nitrogen, and oxygen atom distances from the Ln^{3+} ion. The RDFs for the different Ln^{3+} ions bound to the same ligand ($EDTA^{4-}$), at 25 °C, are plotted together in Fig. 2 to compare how distances change across the Ln series. As expected, due to the Ln ionic radius contraction, Ln–O and Ln–N distances become smaller as the Ln^{3+} ion becomes heavier. Interestingly, the Ln–C distances follow the same trend, indicating that the whole $EDTA^{4-}$ ligand comes closer to the Ln^{3+} ion along the Ln series. Only a single Ln–C peak is observed, even though there are two types of carbon atoms: carboxylate and tertiary amine. This trend is also confirmed by the second peak in the Ln–O RDF, which corresponds to the unbound O atom in the monodentate-bound carboxylate groups.

To determine how varying ligand ($EDTA^{4-}$, $HEDTA^{3-}$) affects the solution structure of Ln–ligand complexes, the La–O, La–N, and La–C RDFs of the $[La^{3+}–EDTA^{4-}\cdot(H_2O)_3]^-$ and $[La^{3+}–HEDTA^{3-}\cdot(H_2O)_4]^0$ complexes at 25 °C are plotted in Fig. 3. While the Ln–O RDF was not significantly affected, the Ln–N RDF changed from a single peak ($EDTA^{4-}$) to two peaks ($HEDTA^{3-}$) as a result of the La-coordinated and uncoordinated N atoms. The Ln–C RDF also changed with the increased flexibility of the uncoordinated $HEDTA^{3+}$ amine yielding a broader distribution compared to $EDTA^{4-}$, and two peaks observed as expected for the different (carboxylate or amine) carbon types.

3.2. Relative binding energies of Ln–EDTA complexes

For a given ligand ($EDTA^{4-}$), Table 1 demonstrates that the experimental relative binding energies follow a trend of increasing binding strength for heavier lanthanides. Using eqn (1) the binding energies of Eu^{3+}, Gd^{3+}, and Lu^{3+} with $EDTA^{4-}$ were computed and compared to that of La^{3+} with $EDTA^{4-}$. The results (Table 1) followed this qualitative trend with errors between experiment and computation (eqn (4)) of 10%, 12%, and 13%, respectively. For a given Ln^{3+} ion (La^{3+}), using eqn (2), the binding energy of $HEDTA^{3-}$ to La^{3+} was compared to that of $EDTA^{4-}$ with La^{3+}, and a 2% error was found between experiment and computation (Table 1).

While it is known that Ln^{3+} ions bind with EDTA much stronger at pH ~11 than at pH ~7, and that for $EDTA^{4-}$ slightly stronger binding is observed along the Ln series, in this work the same trends were predicted solely from computation, without fitting parameters. By comparing the RDFs with the binding behavior, observations can be made on how changes in the solution structure result in different binding energies. From Fig. 2, for a given ligand, complexes with slightly stronger binding energies are observed to have Ln–O, Ln–N, and Ln–C peaks at smaller radial distances. As with the Ln^{3+} aqua ions, the coordination number of Ln–ligand complexes changes from 9 to 8 as the Ln^{3+} ion becomes smaller. However, the bound ligand allows Eu^{3+} and Gd^{3+} to remain 9-coordinate at

 This journal is © the Owner Societies 2022

Published on 05 April 2022. Downloaded by University of Nevada - Reno on 5/20/2022 1:02:28 AM.

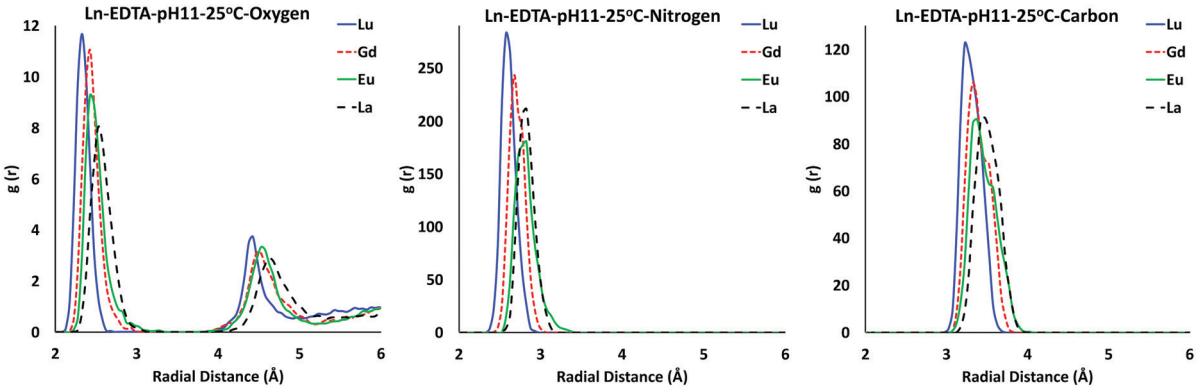

Fig. 2 Radial distribution functions of the $[La^{3+}–EDTA^{4-}\cdot(H_2O)_3]^-$, $[Eu^{3+}–EDTA^{4-}\cdot(H_2O)_3]^-$, $[Gd^{3+}–EDTA^{4-}\cdot(H_2O)_3]^-$, and $[Lu^{3+}–EDTA^{4-}\cdot(H_2O)_2]^-$ complexes at 25 °C. Left, center, and right figures show the Ln–O, Ln–N, and Ln–C pair distribution functions, respectively.

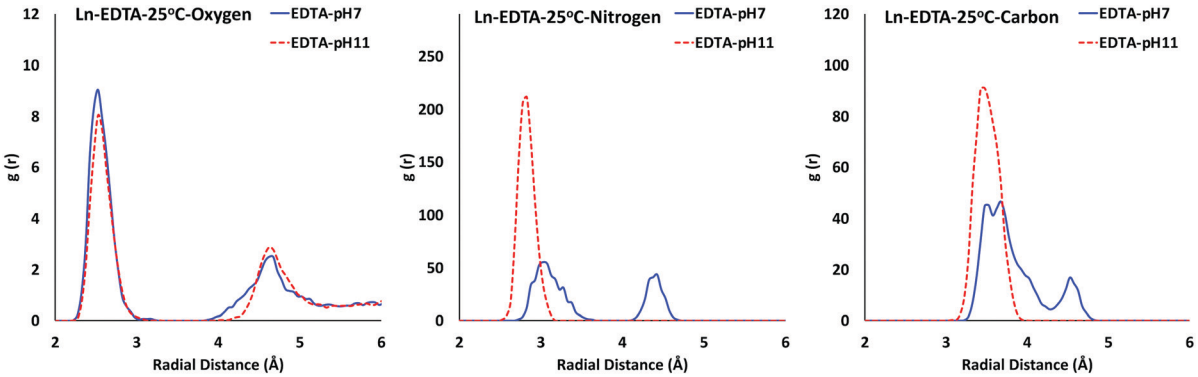

Fig. 3 Radial distribution functions of the $[La^{3+}–HEDTA^{3-}\cdot(H_2O)_4]^-$ complex (pH ~7) and $[La^{3+}–EDTA^{4-}\cdot(H_2O)_3]^-$ complex (pH ~11) at 25 °C. Left, center, and right figures show the La–O, La–N, and La–C pair distribution functions, respectively.

Table 1 Stability constants from experiment and calculated binding energies

Complex	Experimental stability constants[a]	Relative free energy of binding from experiment[b]	Relative binding energy from computation[c]	$\varepsilon_{exp\text{-}comp}$
$[La^{3+}–HEDTA^{3-}\cdot(H_2O)_4]^0$	2.24	0.14	0.12	2%
$[La^{3+}–EDTA^{4-}\cdot(H_2O)_3]^-$	15.46	1 (reference)	1 (reference)	—
$[Eu^{3+}–EDTA^{4-}\cdot(H_2O)_3]^-$	17.32	1.12	1.22	10%
$[Gd^{3+}–EDTA^{4-}\cdot(H_2O)_3]^-$	17.35	1.12	1.25	13%
$[Lu^{3+}–EDTA^{4-}\cdot(H_2O)_2]^-$	19.80	1.28	1.40	12%

[a] log(K) values at 25 °C, from A.E. Martell and Robert M. Smith, "Critical Stability Constants", 1974, Plenum Press, New York. [b] The free energies of binding were calculated from the stability constants with eqn (3). [c] The binding energy for $[La^{3+}–HEDTA^{3-}\cdot(H_2O)_4]^0$ was obtained with the thermodynamic integration in eqn (2), while the remaining binding energies with eqn (1).

25 °C, while for their aqua ions the 8-coordinate state is more likely.[39]

By comparing the solution structures of the $[La^{3+}–EDTA^{4-}\cdot(H_2O)_3]^-$ and $[La^{3+}–HEDTA^{3-}\cdot(H_2O)_4]^0$ complexes, and RDFs in Fig. 3, it was found that lower complex stability correlates with increased ligand/solvent disorder in the Ln–ligand complex. The much stronger binding energy with $EDTA^{4-}$, evidenced by a more rigid ligand structure (sharper Ln–O, Ln–N, and Ln–C peaks), is coupled with the chelate effect of having both nitrogen atoms bound resulting in fewer coordinating water molecules. The weaker binding to $HEDTA^{3-}$, shown by broader Ln–O, Ln–N, and Ln–C peaks, comes with a more disordered bound ligand in the complex with an additional coordinated water molecule. Aside from the fact that the La^{3+} first sphere changed from an N-coordination site from the ligand (in the $[La^{3+}–EDTA^{4-}\cdot(H_2O)_3]^-$ complex) to an O-coordination site from the solvent (in the $[La^{3+}–HEDTA^{3-}\cdot(H_2O)_4]^0$ complex), the geometry of the first coordination sphere does not deviate much when going from pH ~11 to pH ~7. This is seen in: (i) very similar Ln–O RDFs in Fig. 3, (ii)

Published on 05 April 2022. Downloaded by University of Nevada - Reno on 5/20/2022 1:02:28 AM.

in both complexes La^{3+} is 9-coordinate, and (iii) RMSD values to ideal geometries are within the standard deviations, with 0.53 ± 0.8 Å and 0.58 ± 0.8 Å to an ideal tricapped trigonal prism geometry, and 0.47 ± 0.8 Å and 0.57 ± 0.8 Å to an ideal capped square antiprism geometry, for the $[La^{3+}–HEDTA^{3-}\cdot(H_2O)_4]^0$ and $[La^{3+}–EDTA^{4-}\cdot(H_2O)_3]^-$ complexes respectively. Therefore, the significant change in binding energy between the $[La^{3+}–EDTA^{4-}\cdot(H_2O)_3]^-$ and $[La^{3+}–HEDTA^{3-}\cdot(H_2O)_4]^0$ complexes, evidenced by bound-ligand rigidity in the solution structure, comes from an additional ligand N-binding site coupled with the chelate effect, whose binding behavior can be altered with solution pH.

3.3. Effect of temperature on Ln–EDTA complex structure in solution

Simulations were performed at 90 °C of the $[La^{3+}–HEDTA^{3-}\cdot(H_2O)_n]^0$ complex (pH ~7), as well as the $[La^{3+}–EDTA^{4-}\cdot(H_2O)_3]^-$ and $[Lu^{3+}–EDTA^{4-}\cdot(H_2O)_2]^-$ complexes (pH ~11), to determine how temperature affects the solution structure of Ln–ligand complexes with different stabilities. Most notably, the weaker binding $[La^{3+}–HEDTA^{3-}\cdot(H_2O)_n]^0$ complex changed coordination number from 9 to 8 because a water molecule left the first coordination sphere at the higher temperature (n = 4 at 25 °C and n = 3 at 90 °C), while the coordination number did not change for the complexes at pH ~11 with stronger binding. Therefore, ligand binding strength affects the temperature-induced disorder of the first coordination sphere, as well as the binding strength of coordinated solvent molecules in Ln–EDTA complexes.

The Ln–O, Ln–N, and Ln–C RDFs at 25 °C and 90 °C are plotted on the same graph for each complex in Fig. 4 to illustrate how each Ln–EDTA complex changed with temperature in solution. The complexes with relatively larger stability constants appear to have minuscule changes in their RDFs between 25 °C and 90 °C, while the RDFs of the $[La^{3+}–HEDTA^{3-}\cdot(H_2O)_n]^0$ complex with weaker binding changed more significantly with temperature, especially the Ln–N and Ln–C RDFs. This demonstrates that complexed ligands with greater stability

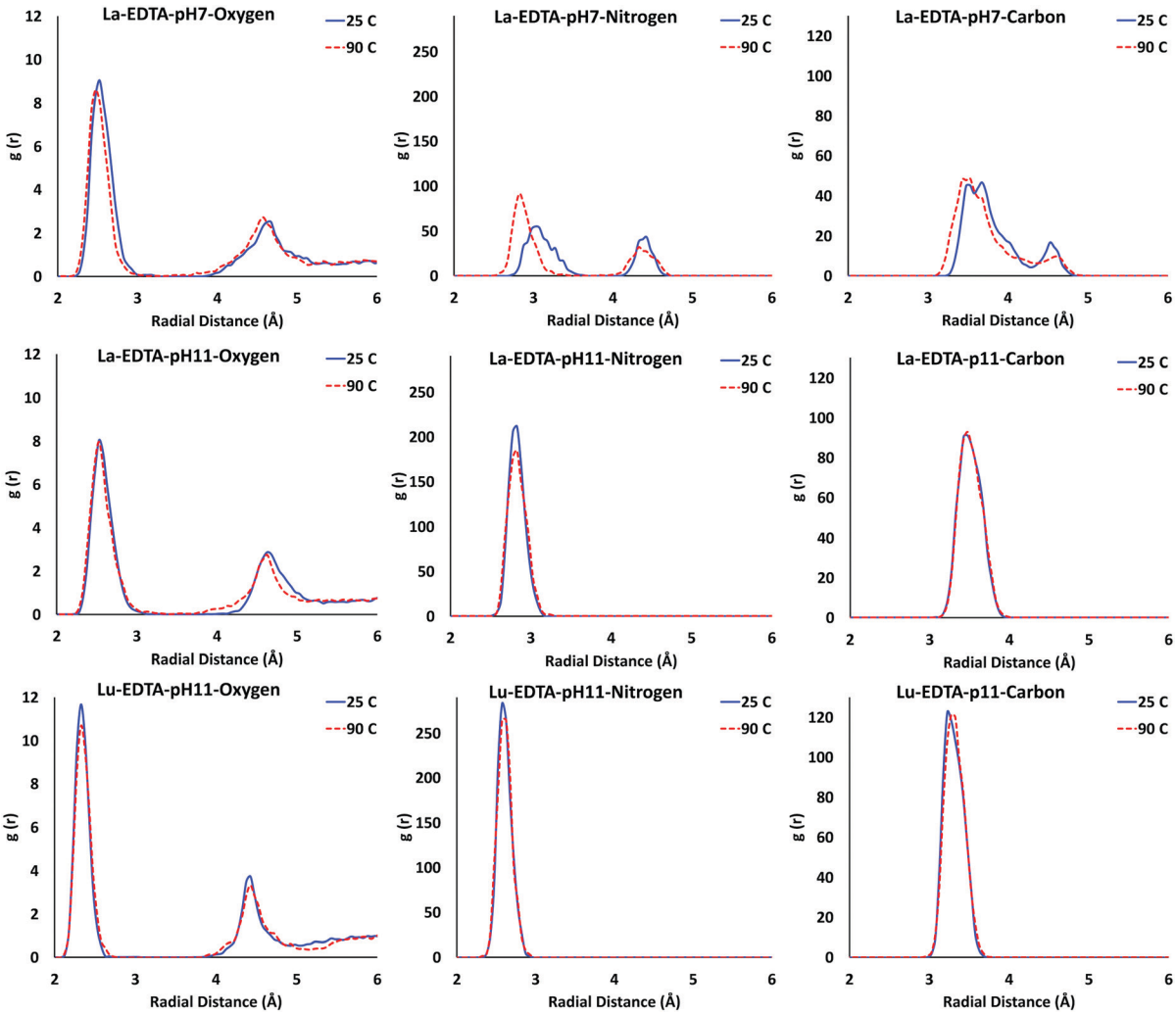

Fig. 4 Radial distribution functions of the $[La^{3+}–HEDTA^{3-}\cdot(H_2O)_n]^0$, $[La^{3+}–EDTA^{4-}\cdot(H_2O)_3]^-$, and $[Lu^{3+}–EDTA^{4-}\cdot(H_2O)_2]^-$ complexes, shown in descending order, at 25 °C and 90 °C. Left, center, and right figures show the Ln–O, Ln–N, and Ln–C pair distribution functions, respectively.

 This journal is © the Owner Societies 2022

Published on 05 April 2022. Downloaded by University of Nevada - Reno on 5/20/2022 1:02:28 AM.

remain more rigid in solution when the temperature increases, however, weaker bound ligands are more susceptible to change their conformation in solution with higher temperatures. Notably, the Ln–N RDFs at 25 °C and 90 °C of the $[La^{3+}$–$HEDTA^{3-}\cdot(H_2O)_n]^0$ complex (Fig. 4, top row) appear counter-intuitive in that the peak is sharper at the higher temperature; this behavior is explained by the fact that the coordination number of the complex changed from 9 (25 °C) to 8 (90 °C).

Ln–O RDFs exhibited very small changes with temperature (Fig. 4), even for the $[La^{3+}$–$HEDTA^{3-}\cdot(H_2O)_n]^0$ complex where the small change is the result of the coordination number change between 90 °C and 25 °C, as was observed with the Ln aqua ions where the temperature-induced disorder decreased along the Ln series.[33] In the Ln^{3+} aqua ions, increasing from 25 °C to 90 °C resulted in a change in coordination number of the earlier Ln elements (Ce^{3+}, Sm^{3+}) but not in the Lu^{3+} aqua ion; a similar behavior is observed in La^{3+} with a weakly-bound ligand ($HEDTA^{3-}$) but not in La^{3+} with a stronger-binding ligand ($EDTA^{4-}$) that stabilizes the entire complex keeping coordinated water molecules in the first shell of the Ln–ligand complex. For the Lu^{3+} ion, both the aqua ion and complex with $EDTA^{4-}$ remained 8-coordinate and retained their first coordination sphere geometry, as shown with RMSD values to ideal geometries between the two temperatures that are within their standard deviation: 0.39 ± 0.06 Å and 0.40 ± 0.05 Å for the bicapped trigonal prismatic geometry; 0.41 ± 0.08 Å and 0.39 ± 0.07 Å for the square antiprism; and 0.29 ± 0.04 Å and 0.33 ± 0.07 Å for the dodecahedral geometry; at 25 °C and 90 °C respectively. Although the Lu^{3+} aqua ion favors the square antiprism geometry at 25 °C,[41] and the dodecahedral geometry at 90 °C,[33] the Lu^{3+} ion favors the dodecahedral geometry at both temperatures in complex with $EDTA^{4-}$ revealing ligand stabilization of the first Lu^{3+} coordination sphere.

4. Conclusions

AIMD simulations were used to characterize the solution structures of EDTA complexed with Ln^{3+} ions in two different pH conditions and temperatures. Radial pair distributions for the Ln^{3+}–$EDTA^{4-}$ complexes, corresponding to pH ~11, confirm that as the Ln^{3+} ionic radius decreases, Ln^{3+}–O/N bonds shorten and the number of coordinated water molecules decreases from three (for the La^{3+}, Eu^{3+}, Gd^{3+} ions) to two (for the Lu^{3+} ion). The trend in thermodynamic stability for Ln^{3+}–$EDTA^{4-}$ was reproduced in the relative binding energies computed with electronic structure calculations. Protonating an amine nitrogen atom of $EDTA^{4-}$ to form $HEDTA^{3-}$, as a result of changing from pH ~11 to pH ~7, prevented Ln–nitrogen coordination without significant effect on the coordinated carboxylate groups; instead, an additional water molecule coordinated to the complex to maintain the same coordination number. Nevertheless, the thermodynamic stability of the La^{3+}–$HEDTA^{3-}$ complex, corresponding to pH ~7, was greatly reduced compared to that of the La^{3+}–$EDTA^{4-}$ complex, corresponding to pH ~11. This relative difference was reproduced by calculating relative binding energies. The reported Ln^{3+}–$EDTA^{4-}$ structures agree with previous studies, and the reported structure of the La^{3+}–$HEDTA^{3-}$ complex shows the structural basis of how solution pH can change complex stability constants. Regarding temperature, while the solution structures of Ln^{3+}–$EDTA^{4-}$ complexes did not change significantly upon increasing from 25 °C to 90 °C, a water from La^{3+}–$HEDTA^{3-}$ detached and the complex changed from a nine coordinate structure to an eight coordinate structure, similar to what has been previously observed for lanthanide aqua complexes. Furthermore, this work provides an avenue for predicting relative lanthanide–ligand stabilities in the absence of experimental data.

Conflicts of interest

There are no conflicts to declare.

Acknowledgements

Support from the National Science Foundation (Award 2041914). This material is based upon work supported by the U.S. Department of Energy, Office of Science, Office of Basic Energy Sciences under Award Number DE-SC0022178. Calculations and simulations were performed in Pronghorn, the High-Performance Computing cluster of the University of Nevada, Reno.

References

1 B. Kronholm, C. G. Anderson and P. R. Taylor, A primer on hydrometallurgical rare earth separations, *JOM*, 2013, **65**, 1321–1326.
2 N. Krishnamurthy and C. K. Gupta, *Extractive Metallurgy of Rare Earths*, CRC Press, 2nd edn, 2016.
3 R. M. Smith and A. E. Martell, *Critical stability constants*, Plenum Press, 1974, vol. 1.
4 B. W. McCann, N. De Silva, T. L. Windus, M. S. Gordon, B. A. Moyer, V. S. Bryantsev and B. P. Hay, Computer-aided molecular design of bis-phosphine oxide lanthanide extractants, *Inorg. Chem.*, 2016, **55**, 5787–5803.
5 M. N. Vo, V. S. Bryantsev, J. K. Johnson and J. A. Keith, Quantum chemistry benchmarking of binding and selectivity for lanthanide extractants, *Int. J. Quantum Chem.*, 2018, **118**, e25516.
6 G. A. McCarver, R. J. Hinde and K. D. Vogiatzis, Selecting Quantum-Chemical Methods for Lanthanide-Containing Molecules: A Balance between Accuracy and Efficiency, *Inorg. Chem.*, 2020, **59**, 10492–10500.
7 K. Niu, F. Yang, T. Gaudin, H. Ma and W. Fang, Theoretical Study of Effects of Solvents, Ligands, and Anions on Separation of Trivalent Lanthanides and Actinides, *Inorg. Chem.*, 2021, **60**, 9552–9562.
8 M. L. Free, *Hydrometallurgy*, Wiley, 2013.

Published on 05 April 2022. Downloaded by University of Nevada - Reno on 5/20/2022 1:02:28 AM.

9 F. Xie, T. A. Zhang, D. Dreisinger and F. Doyle, A critical review on solvent extraction of rare earths from aqueous solutions, *Miner. Eng.*, 2014, **56**, 10–28.
10 D. C. Cantu, Predicting lanthanide coordination structures in solution with molecular simulation, in *Methods in Enzymology*, ed. J. A. Cotruvo Jr., Academic Press, 2021, vol. 651, pp. 193–233.
11 D. S. Kaliakin, J. A. Sobrinho, J. H. S. K. Monteiro, A. de Bettencourt-Dias and D. C. Cantu, Solution structure of a europium–nicotianamine complex supports that phytosiderophores bind lanthanides, *Phys. Chem. Chem. Phys.*, 2021, **23**, 4287–4299.
12 R. C. Shiery, K. A. Cooper and D. C. Cantu, Computational Prediction of All Lanthanide Aqua Ion Acidity Constants, *Inorg. Chem.*, 2021, **60**, 10257–10266.
13 M. Douglas and N. M. Kroll, Quantum electrodynamical corrections to the fine structure of helium, *Ann. Phys.*, 1974, **82**, 89–155.
14 B. A. Hess, Applicability of the no-pair equation with free-particle projection operators to atomic and molecular structure calculations, *Phys. Rev. A: At., Mol., Opt. Phys.*, 1985, **32**, 756–763.
15 D. A. Pantazis, X. Y. Chen, C. R. Landis and F. Neese, All-electron scalar relativistic basis sets for third-row transition metal atoms, *J. Chem. Theory Comput.*, 2008, **4**, 908–919.
16 J. Zheng, X. Xu and D. G. Truhlar, Minimally augmented Karlsruhe basis sets, *Theor. Chem. Acc.*, 2011, **128**, 295–305.
17 D. E. Woon and T. H. Dunning, Gaussian basis sets for use in correlated molecular calculations. I. The atoms boron through neon and hydrogen, *J. Chem. Phys.*, 1988, **90**, 1007–1023.
18 F. Weigend and R. Ahlrichs, Balanced basis sets of split valence, triple zeta valence and quadruple zeta valence quality for H to Rn: Design and assessment of accuracy, *Phys. Chem. Chem. Phys.*, 2005, **7**, 3297–3305.
19 N. Mardirossian and M. Head-Gordon, How Accurate Are the Minnesota Density Functionals for Noncovalent Interactions, Isomerization Energies, Thermochemistry, and Barrier Heights Involving Molecules Composed of Main-Group Elements?, *J. Chem. Theory Comput.*, 2016, **12**, 4303–4325.
20 S. Grimmel, G. Schoendorff and A. K. Wilson, Gauging the Performance of Density Functionals for Lanthanide-Containing Molecules, *J. Chem. Theory Comput.*, 2016, **12**, 1259–1266.
21 A. Jaoul, G. Nocton and C. Clavaguéra, Assessment of Density Functionals for Computing Thermodynamic Properties of Lanthanide Complexes, *ChemPhysChem*, 2017, **18**, 2688–2696.
22 M. Dolg, *Computational methods in lanthanide and actinide chemistry*, Wiley, 2015.
23 F. E. Jorge, L. S. C. Martins and M. L. Franco, All-electron double zeta basis sets for the lanthanides: Application in atomic and molecular property calculations, *Chem. Phys. Lett.*, 2016, **643**, 84–88.
24 A. Z. de Oliveira, I. B. Ferreira, C. T. Campos, F. E. Jorge and P. A. Fantin, Segmented all-electron basis sets of triple zeta quality for the lanthanides: application to structure calculations of lanthanide monoxides, *J. Mol. Model.*, 2019, **25**, 38.
25 D. Aravena, F. Neese and D. A. Pantazis, Improved Segmented All-Electron Relativistically Contracted Basis Sets for the Lanthanides, *J. Chem. Theory Comput.*, 2016, **12**, 1148–1156.
26 Y. Zhao and D. G. Truhlar, The M06 suite of density functionals for main group thermochemistry, thermochemical kinetics, noncovalent interactions, excited states, and transition elements: Two new functionals and systematic testing of four M06-class functionals and 12 other function, *Theor. Chem. Acc.*, 2008, **120**, 215–241.
27 T. H. Dunning, Gaussian basis sets for use in correlated molecular calculations. I. The atoms boron through neon and hydrogen, *J. Chem. Phys.*, 1989, **90**, 1007–1023.
28 V. Barone and M. Cossi, Quantum calculation of molecular energies and energy gradients in solution by a conductor solvent model, *J. Phys. Chem. A*, 1998, **102**, 1995–2001.
29 F. Neese, Software update: the ORCA program system, version 4.0, *Wiley Interdiscip. Rev.: Comput. Mol. Sci.*, 2018, **8**, 4–9.
30 F. Neese, F. Wennmohs, A. Hansen and U. Becker, Efficient, approximate and parallel Hartree-Fock and hybrid DFT calculations. A 'chain-of-spheres' algorithm for the Hartree-Fock exchange, *Chem. Phys.*, 2009, **356**, 98–109.
31 N. Sakagami, Y. Yamada, T. Konno and K. I. Okamoto, Crystal structures and stereochemical properties of lanthanide(III) complexes with ethylenediamine-N,N,N′,N′-tetraacetate, *Inorg. Chim. Acta*, 1999, **288**, 7–16.
32 J. N. Mathur, P. Thakur, C. J. Dodge, A. J. Francis and G. R. Choppin, Coordination modes in the formation of the ternary Am(III), Cm(III), and Eu(III) complexes with EDTA and NTA: TRLFS, 13C NMR, EXAFS, and thermodynamics of the complexation, *Inorg. Chem.*, 2006, **45**, 8026–8035.
33 D. M. Driscoll, R. C. Shiery, M. Balasubramanian, J. L. Fulton and D. C. Cantu, Ionic Contraction across the Lanthanide Series Decreases the Temperature-Induced Disorder of the Water Coordination Sphere, *Inorg. Chem.*, 2022, **61**, 287–294.
34 J. P. Perdew, K. Burke and M. Ernzerhof, Generalized Gradient Approximation Made Simple, *Phys. Rev. Lett.*, 1996, **77**, 3865–3868.
35 J. B. Lu, D. C. Cantu, M. T. Nguyen, J. Li, V. A. Glezakou and R. Rousseau, Norm-Conserving Pseudopotentials and Basis Sets to Explore Lanthanide Chemistry in Complex Environments, *J. Chem. Theory Comput.*, 2019, **15**, 5987–5997.
36 J. Hutter, M. Iannuzzi, F. Schiffmann and J. VandeVondele, CP2k: Atomistic simulations of condensed matter systems, *Wiley Interdiscip. Rev.: Comput. Mol. Sci.*, 2014, **4**, 15–25.
37 J. VandeVondele and J. Hutter, Gaussian basis sets for accurate calculations on molecular systems in gas and condensed phases, *J. Chem. Phys.*, 2007, **127**, 114105.
38 S. Grimme, J. Antony, S. Ehrlich and H. Krieg, A consistent and accurate ab initio parametrization of density functional dispersion correction (DFT-D) for the 94 elements H-Pu, *J. Chem. Phys.*, 2010, **132**, 154104.

 This journal is © the Owner Societies 2022

39 R. C. Shiery, J. L. Fulton, M. Balasubramanian, M.-T. Nguyen, J.-B. Lu, J. Li, R. Rousseau, V.-A. Glezakou and D. C. Cantu, Coordination Sphere of Lanthanide Aqua Ions Resolved with Ab Initio Molecular Dynamics and X-ray Absorption Spectroscopy, *Inorg. Chem.*, 2021, **60**, 3117–3130.
40 S. Durand, J. P. Dognon, P. Guilbaud, C. Rabbe and G. Wipff, Lanthanide and alkaline-earth complexes of EDTA in water: a molecular dynamics study of structures and binding selectivities, *J. Chem. Soc., Trans.*, 2000, **2**, 705–714.
41 B. Qiao, S. Skanthakumar and L. Soderholm, Comparative CHARMM and AMOEBA Simulations of Lanthanide Hydration Energetics and Experimental Aqueous-Solution Structures, *J. Chem. Theory Comput.*, 2018, **14**, 1781–1790.

Published on 05 April 2022. Downloaded by University of Nevada - Reno on 5/20/2022 1:02:28 AM.